JCTC Journal of Chemical Theory and Computation

Article

pubs.acs.org/JCTC

Spin-Crossing in an Organometallic Pt−Benzene Complex

Jaroslav Granatier,[†,∥] Matúš Dubecký,[‡,§,∥] Petr Lazar,[‡] Michal Otyepka,*[,‡] and Pavel Hobza*[,†,‡]

[†]Institute of Organic Chemistry and Biochemistry, Academy of Sciences of the Czech Republic, Flemingovo nám. 2, 166 10 Prague 6, Czech Republic

[‡]Regional Centre of Advanced Technologies and Materials, Department of Physical Chemistry, Faculty of Science, Palacký University Olomouc, tř. 17. listopadu 12, 771 46 Olomouc, Czech Republic

[§]Institute of Electrical Engineering, Slovak Academy of Sciences, Dúbravská cesta 9, 841 04 Bratislava, Slovakia

ABSTRACT: The interaction between the Pt atom and the benzene (Bz) molecule was investigated theoretically, using a symmetric Pt−Bz half-sandwich complex. Various levels of wave function theory (HF, MP2, CCSD(T), CASPT2, multistate (MS) MS-CASPT2) together with several functionals (PBE, PBE+D3, PBE+vdW, PBE/EE+vdW) of the density functional theory (DFT) were complemented by quantum Monte Carlo (QMC) calculations. Spin−orbit coupling (SOC) effects were also taken into account at the CASPT2 and DFT levels of theory. The inclusion of dynamic correlation energy was found to be essential to maintaining the stability of the complex. The dative type of bonding was identified to be responsible for the Pt−Bz binding in the ground state. Single-reference CCSD(T) and MP2 as well as multireference CASPT2 and MS-CASPT2 methods reveal that the interaction curve has a single energy minimum (corresponding to the $^1S_0$ state) and a shoulder (arising from the crossing between the $^1S_0$ and $^3D_3$ states) at longer distances. The inclusion of SOC at the CASPT2 level leads to the appearance of another well-separated minimum, which corresponds to the triplet state $^3F_4$. The PBE/EE+vdW functional, which includes a fraction of exact-exchange (EE) and nonlocal electron correlation, shows the best qualitative agreement with respect to the CCSD(T) data among all DFT functionals used. Large-scale QMC calculations, based on DFT wave functions constructed using TPSSh and M11 functionals, were confronted with the CCSD(T) results. The QMC-TPSSh protocol favorably agrees with the CCSD(T) data, suggesting its possible use in other Pt-containing organometallic systems. All of the methods used (except for HF) show that the Pt−benzene binding leads to the quenching of the Pt high-spin triplet ground state, and the low-spin closed-shell singlet state is found to be preferred in the ground-state of the complex.

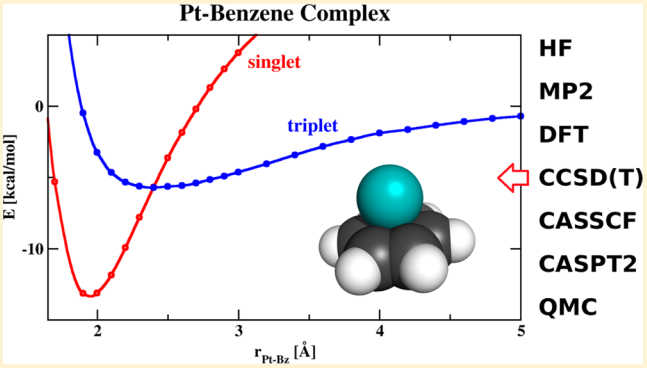

INTRODUCTION

The adsorption of aromatic molecules on metal surfaces is an important process in surface science,[1] catalysis,[2,3] molecular electronics,[4] and spintronics.[5,6] Theoretical calculations can provide essential understanding of the nature of binding between various aromatic adsorbates and metals. The metal surfaces are usually studied in terms of the density functional theory (DFT),[7] formulated within the periodic boundary conditions. The description of the adsorption properties however suffers from the intrinsic limitations of conventional DFT functionals (based on the local density approximation or generalized gradient approximation), in particular the electron self-interaction error and a poor description of the nonlocal electron−electron correlation effects.[7−10] The latter problem has led to a rapid development of nonlocal DFT exchange-correlation (xc) functionals, which has included nonlocal terms and provided some promising results for the interaction between metals and aromatics (e.g., vdW-DF,[11] PBE+vdWsurf,[12] optB88-vdW,[13] or EE+vdW[14,15]). In this respect, a recent DFT study of the interaction between the Pt(111) surface and molecular benzene[13] has reported two interesting findings. First, two minima on the interaction energy curve between the Pt(111) surface and molecular benzene were identified, in accord with the experiment indicating the existence of a precursor physisorption state for the benzene adsorbing on the Pt(111) surface.[16] The precursor state implies that the potential-energy curve has indeed a double-well shape, which is very rare on metal surfaces. Second, it was suggested that the van der Waals corrections can trigger binding from physisorption to weak chemisorption, changing the nature of binding qualitatively.[13] Nevertheless, there are several important effects such as the multireference nature of the many-body wave function, dynamic electron correlation effects, and the spin−orbit coupling (SOC),[17,18] which can mediate the Pt−benzene interaction but go beyond the realm of the DFT method, as used e.g. in ref 13.

Received: January 7, 2013
Published: February 15, 2013

On the other hand, it is possible to treat these effects accurately and consistently using wave function theory (WFT) and/or quantum Monte Carlo (QMC) methods. The system size, accessible to the advanced quantum mechanical (QM) methods, is however fairly limited due to their enormous computational cost. The simplest possible model of the metal−benzene interaction, allowing the use of high-level methods, consists of a single metal atom attached to a benzene ring. Such systems belong to the more general class known as transition metal−arene (TM−arene) complexes. They are of importance[19] for their (potential) applications in organic/organometallic synthesis,[20,21] catalysis,[22] nanotechnology,[23,24] and spintronics.[25,26] Recently, Błoński and Hafner[27,28] have found in their DFT study that the spin of the Pt atoms adsorbed on graphene is quenched, which again calls for a detailed understanding of Pt atom−arene interactions.

In this paper, we study a Pt−benzene (Pt−Bz) half-sandwich TM−arene complex using WFT, DFT, and QMC techniques. Specifically, we apply conventional single-reference (HF, MP2, CCSD(T)) and multireference (CASSCF, CASPT2) methods. The performance of various vdW corrections is tested within the DFT framework (empirical DFT-D3 and nonlocal vdW-DF functional). In addition, large-scale QMC calculations based on DFT trial wave functions are performed in order to compare the results against CCSD(T).

The aim of the study is two-fold: first, to explore the potential-energy surfaces of the system considered using the above-mentioned methods, and second, to explain the nature of the secondary weak minimum identified. Notice that a proper description of the electronic structure of a Pt atom is a complicated task, namely because of the presence of nearly degenerate electronic states. The ground state of the atom is the triplet, $^3D_3$, with a valence electron configuration of $5d^96s^1$. The first excited open-shell singlet ($^1D_2$) possesses the same electron configuration, lying only 2.2 kcal/mol above the ground state. The second excited state with an excitation energy of 2.4 kcal/mol corresponds to the triplet state ($^3F_4$) with a configuration of $5d^86s^2$. The third excited state is a closed-shell singlet ($^1S_0$) with an electron configuration of $5d^{10}6s^0$. Despite the fact that its excitation energy is much higher (17.6 kcal/mol) in comparison with the mentioned lower states, this state is highly interesting from a theoretical point of view. The closed-shell singlet is the dominant configuration of a Pt atom in the ground state of the Pt−Bz complex. Interestingly, its valence electron configuration, $5d^{10}6s^0$, is similar to the configuration of the Pd-atom ground state ($4d^{10}5s^0$). In our previous study,[14] we demonstrated that in the ground state a Pd atom forms a strong dative bond with the carbon atoms of a benzene ring. Analogically, it is possible that a Pt atom with the same configuration participates in the Pt−Bz bonding in a similar way.

We found that d−π interactions between Pt and benzene preferentially stabilize the singlet ground state at short distances, whereas at medium distances, the spin-crossing occurs as the Pt atom approaches its $^3D_3$ ground state (henceforth, we classify electronic states of Pt−Bz complex using the Pt atom states). Contrary to single-reference methods, multiconfigurational methods (multistate (MS) CASPT2/CASPT2-SO) reveal a second minimum on the dissociation profile. The nature of the secondary minimum is explained by the subtle interplay of SOC and electronic correlation, which promotes the $^3F_4$ state below the $^3D_3$ state at intermediate distances. This effect arises from the multireference nature of the Pt−Bz wave function, which cannot be properly described by such single reference methods as DFT or CCSD(T).

The DFT results reveal only a limited consensus regarding the position of the minima and the relative energy differences, demonstrating their limited predictive power in d-block organometallics if used without prior benchmarking.[14,15,30,31] The DFT-D3 technique shows a shoulder at a single-minimum energy curve, explained by the nonmonotonous nature of the damping function for the dispersion energy correction. The PBE/EE+vdW approach, containing a fraction of exact-exchange (EE) and nonlocal electron correlation, shows the best qualitative agreement as compared to the CCSD(T) data from the set of the xc functionals used. Finally, large-scale QMC calculations based on wave functions constructed using modern xc functionals, TPSSh and M11, were performed in order to benchmark the results against CCSD(T). Using a fine step size, we obtained full energy-distance curves, providing valuable non-routine[32] insight into the performance of the QMC in organometallic d−π interactions. The QMC-TPSSh protocol favorably agrees with the reference data, suggesting its viable use in other (related) Pt-containing organometallic systems.

COMPUTATIONAL DETAILS

The single- and multireference WFT and DFT methods were used to calculate the structure and interaction energy of the Pt−Bz complex as well as to investigate the nature of bonding in it. The two different single-reference WFT approaches used include the spin-adapted CCSD(T) method with restricted closed-/open-shell Hartree−Fock (HF) reference functions[33−36] and the less demanding MP2 method.[37] The multireference Complete Active Space SCF (CASSCF) method,[38] the pertubative correlation analogue (CASPT2),[39−41] and its multistate extension (MS-CASPT2)[42] methods recovering dynamic correlation energy were also utilized. The standard IPEA shift[43] (0.25 au) has been used in all of our CASPT2 calculations. The $5p^65d^96s^1$ shells of platinum and all electrons in benzene with an exception of the $1s^2$ electrons of the carbon atoms were treated. A resulting active space used thus consists of 16 electrons placed in 12 orbitals (16/12)—10 electrons in six orbitals for the Pt atom (5d and 6s orbitals) and six electrons in six orbitals for benzene (perpendicular to the benzene plane).

SOC effects were estimated using the restricted active space state interaction (RASSI) method within the CASSCF/CASPT2/RASSI-SO approach introduced by Roos and Malmqvist.[44−46] In the present study, 20 and 15 lowest-lying roots of singlet and triplet spin states, respectively, were selected on the basis of calculations performed with a VTZP basis set. The calculations with combined VQZP/VTZP basis sets (see below) were performed with 5 and 12 lowest-lying roots of singlet and triplet spin states, respectively. All these spin states were consequently used in correlated MS-CASPT2 calculations.

All of the WFT calculations were carried out using ANO-RCC basis sets[47,48] containing diffuse and polarization functions and allowing the use of various degrees of contraction. While the MP2 and CCSD(T) calculations were performed with the VTZP contraction, the CASSCF/CASPT2 calculations employed the same contractions as well as their combination, i.e., VQZP (Pt atom)/VTZP (benzene molecule). The scalar relativistic one-component Douglas−Kroll−Hess

approximation was used thoroughly.[49,50] The interaction energies were corrected for the basis set superposition error (BSSE) using the counterpoise correction.[51] The WFT calculations were performed using the MOLCAS 7.2 program package.[52]

The DFT and the DFT-D3[53] calculations, in the Gaussian def2-QZVP[54] basis set, were carried out using the PBE[55,56] xc functional within the GAMESS[57] code. The plane-wave (pw) DFT calculations were performed using the PAW method[58] and the PBE xc functional as implemented in the Vienna Ab initio Simulation Package (VASP).[59] The energy cutoff for the pw expansion of the eigenfunctions was set to 400 eV. The Pt−Bz complex was put into a large supercell (24 × 24 × 24 Å) to minimize the interactions of repeated images. The triplet and singlet states of Pt were fixed during the calculation by constraining the total magnetic moment of the supercell. Long-range van der Waals (dispersion) interactions, which are absent in the standard DFT, were included by means of the van der Waals density functional[11] (denoted as PBE+vdW). The effect of adding exact exchange to the xc mixture was tested[14,15] by the construction of the exchange part of the xc functional, E_x, as a linear combination of the generalized-gradient-approximation exchange, from PBE, and the exact exchange (EE), as $E_x = 3/4E_{PBEx} + 1/4E_{EEx}$ (denoted as EE+vdW).

The effect of SOC was inspected within pw DFT by means of a two-component relativistic Hamiltonian, as implemented in VASP, which contains spin−orbit coupling and all of the relativistic corrections up to the order of α^2 (where α is the fine-structure constant). The presence of spin−orbit coupling gives rise to the Hamiltonian, which does not commute with the spin and orbital momenta. Consequently, the spin is no longer a good quantum number. Therefore, in the case of spin−orbit calculations, the spin moment was allowed to relax, as a result of which the singlet and triplet states were not exactly defined.

The QMC simulations used a multistage approach:[30,60,61] (i) Single-determinant trial wave functions were constructed from DFT, using TPSSh[62] or M11[63] xc functionals, within the GAMESS[57] suite. Nondivergent effective-core potentials[64,65] and valence cc-pVTZ quality basis sets[66] were used on C and H; the Pt was represented by the def2 effective-core potential[67] and the corresponding def2-TZVP basis set.[54] (ii) The parameters of the Schmidt−Moskowitz−Jastrow factor[68,69] in the wave functions of the Slater−Jastrow type were subsequently optimized within the variational Monte Carlo (VMC) in the iterative manner. Electron−nucleus and electron−electron terms, accounting for the explicit dependence of the wave function on the interelectronic distances, were included. The employed trial wave function improvement strategy leads to local-energy variance reductions, whereas the nodal surfaces remain intact and fully rely on the DFT input. (iii) Production energies with a statistical error bar below 0.005 eV were obtained by the fixed-node diffusion Monte Carlo (DMC) imaginary-time projection[70−72] using a time-step of 0.01 au, giving an acceptance ratio of >0.99. All of the VMC and DMC runs were performed using the qwalk[73] code.

There are three high-symmetry adsorption sites of the Pt atom on benzene: the "top," directly above a carbon atom; the "bridge," above the midpoint of a C−C bond; and the so-called "hollow" site, above the center of the aromatic ring. Here, we investigate the hollow structure model because of its high symmetry (C_6). Our calculations for the remaining sites show only small quantitative changes of the adsorption properties (the data not shown). The benzene structure, kept frozen in all calculations, was optimized at the MP2/cc-pVTZ level (C−C and C−H distances were equal to 1.394 Å and 1.082 Å, respectively).

RESULTS AND DISCUSSION

The single-reference HF, MP2, and CCSD(T) approaches (Figure 1) were used for the calculations of the interaction

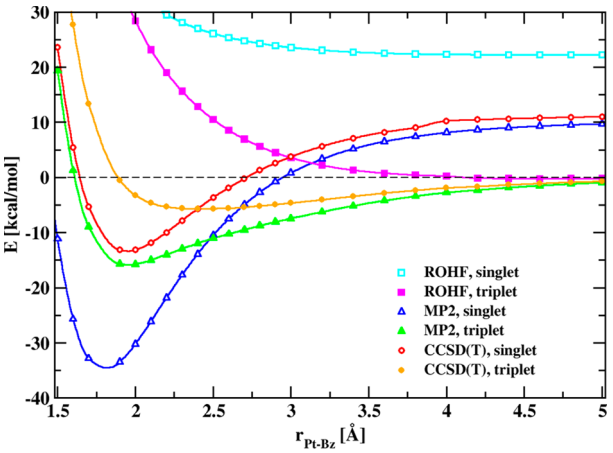

Figure 1. DKH relativistic BSSE-corrected ROHF, MP2, and CCSD(T) potential-energy curves calculated in the ANO-RCC-VQZP/VTZP basis sets for the singlet and triplet states of the Pt−Bz complex, with the metal adsorbed at the hollow position. Note that the energies of the subsystems used for the calculation of the interaction energies correspond to their ground state (i.e., Pt atom, triplet state; benzene molecule, singlet state).

between the Pt atom and benzene in singlet $^1S_0$ and triplet $^3D_3$ states. The HF method provides a repulsive description of this interaction for both states (Figure 1). Passing to single-reference correlated methods, MP2 and CCSD(T), the energy minimum appears (Figure 1), unambiguously demonstrating the decisive role of the dynamic correlation energy in the studied complex. The MP2 binding energies for singlet and triplet states, 34.7 and 15.9 kcal/mol (at 1.80 and 1.95 Å, respectively), are much higher than the CCSD(T) ones, 13.4 and 5.7 kcal/mol (at 1.95 and 2.40 Å, respectively), showing the known tendency of the MP2 method to overestimate the stacking energy.[74,75] Both correlated methods indicate that the singlet state is approximately 2 times more stable than the triplet state and that the Pt−Bz singlet-state minimum distance is shorter than the distance in the case of the triplet state. The crossing of MP2 and CCSD(T) singlet and triplet potential-energy curves occurs at 2.48 and 2.40 Å, respectively, and the stabilization energies corresponding to these distances amount to 11.2 and 5.7 kcal/mol. The difference between the triplet and singlet states in the dissociation limit determined at the MP2 and CCSD(T) levels is approximately 7 and 6 kcal/mol lower than the experimental value of 17.6 kcal/mol.[29,76] The discrepancy is attributable to the consideration of the closed-shell instead of the lower open-shell term and to the neglect of the SOC. On the other hand, the values are close to a state-averaged value of 11.02 kcal/mol[17,29] (Table 1).

The CASSCF/VQZP/VTZP method, analogously to the single-reference HF/VTZP approach, provides only the repulsive interaction energy curves (Figure 2), indicating that the multireference nature of the wave function is not

dx.doi.org/10.1021/ct400016c | J. Chem. Theory Comput. 2013, 9, 1461−1468

Table 1. A Summary of the Results for the Singlet (S) and Triplet (T) States of the Pt−Bz Complex: The Interaction Energies D^S and D^T (kcal/mol), Equilibrium Pt−Bz Distances r^S and r^T (Å), and S−T Level Splittings in the Pt−Bz Dissociation Limit, Δ^{ST}

method/basis set	D^S	r^S	D^T	r^T	Δ^{ST}
MP2/VTZP	34.7	1.80	15.9	1.95	10.4
CCSD(T)/VTZP	13.4	1.95	5.7	2.40	11.2
MS-CASPT2/VQZP+VZTP	36.2	1.86	23.5	1.94	0.7[d]
MS-CASPT2-SO/VQZP+VZTP	26.7	1.87	19.5	1.98	
PBE/pw	19.5	1.94	9.5	2.10	8.3
PBE+vdW/pw	10.4	2.07	6.0	2.50	8.4
PBE-SO/pw	10.3	1.96			
EE+vdW/pw	21.5	2.03	17.2	2.45	21.4
EE+vdW-SO/pw	12.4	2.05[b]	6.4	2.6[c]	
PBE/VQZP	17.4	1.95	8.2	2.18	11.5
PBE+D3/VQZP	18.7	1.97	9.9	2.20	11.5
QMC-M11[a]	11.6(2)	2.00(5)	5.54(1)	2.50(5)	9.4(2)
QMC-TPSSh[a]	12.2(2)	2.00(5)	5.50(1)	2.50(5)	10.9(2)
exptl.					11.02[d]

[a]The error bars of the QMC data are indicated in parentheses. [b]Deep minimum (Figure 6). [c]Weak minimum (Figure 6). [d]j average.[17,29]

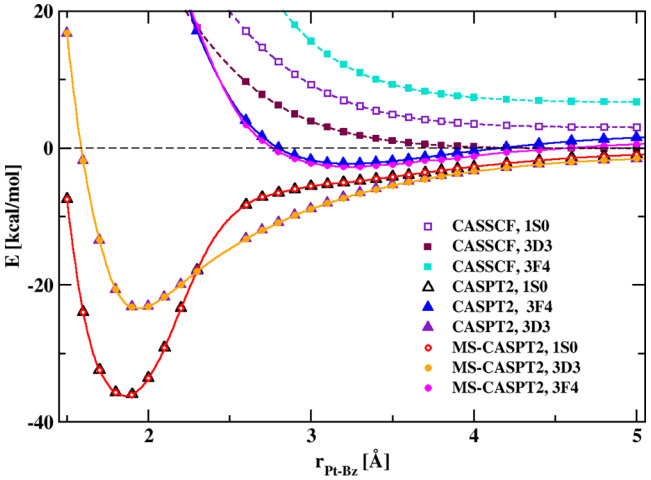

Figure 2. DKH relativistic BSSE-corrected CASSCF, CASPT2, and MS-CASPT2 potential-energy curves calculated in the ANO-RCC-VQZP/VTZP basis sets for the most stable $^1S_0$ and triplet ($^3D_3$ and $^3F_4$) states of the Pt···benzene complex, with the metal adsorbed at the hollow position. The CASPT2 and MS-CASPT2 potential curves are identical for the $^1S_0$ and $^3D_3$ states.

responsible for the stabilization of the complex. When the CASPT2/VQZP/VTZP approach is applied, the single energy minimum appears at singlet and triplet potential curves (Figure 2). The CASPT2/VQZP/VTZP binding energies of the most stable singlet and triplet roots were found to be 36.2 kcal/mol (1.86 Å) and 23.4 kcal/mol (1.94 Å), respectively. These results are closer to the MP2 values than to the CCSD(T) ones (cf. Table 1). The CASPT2 singlet−triplet crossing was detected at 2.29 Å (energy 18.1 kcal/mol), i.e., at a distance slightly shorter than given by MP2 and CCSD(T) (2.48 and 2.40 Å, respectively). The MS-CASPT2 approach provides essentially identical binding energies and positions of the minima (36.2 and 23.5 kcal/mol at 1.86 and 1.94 Å, respectively) and the singlet−triplet crossing (2.29 Å, an energy of 18.1 kcal/mol) as the CASPT2 level (Figure 2). The multireference approaches, like the single-reference ones, prefer the triplet state in agreement with the experiment. The energy gap between the triplet and singlet states in the dissociation limit is only 0.7 kcal/mol at both the CASPT2 and MS-CASPT2 levels, respectively. This value is much lower than that obtained from the single-reference methods mentioned above. Basically, the multireference methods correctly describe the electron configuration of the lowest singlet as the open-shell state $^1D_2$, which is close to the triplet ground state, $^3D_3$. On the other hand, the single-reference methods describe correctly the energy gap between the closed-shell states $^1S_0$ and $^3D_3$, respectively. At the equilibrium distance, the $^1D_2$ state is less stable than the singlet state $^1S_0$. At a longer distance of about 2.78 Å, both states cross. The increase of the intermolecular distance leads to the change of the character of the most stable singlet-state solution. While at the distances near the equilibrium, the singlet ground state is best described as the closed-shell singlet ($^1S_0$); at greater distances, the open-shell singlet ($^1D_2$) state is preferred.

All the above-reported calculations were performed without SOC, which is known to play an important role in heavy transition-metal elements.[46] The inclusion of SOC to MS-CASPT2 calculations reduces the interaction energy of both the $^1S_0$ and $^3D_3$ states, but SOC behaves differently for different spin states (Figure 3). In the case of the $^3D_3$ state, the SOC

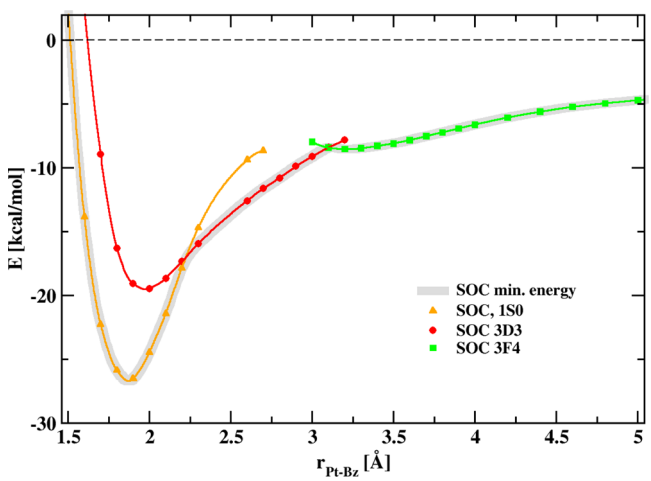

Figure 3. DKH relativistic BSSE-corrected MS-CASPT2-SOC potential-energy curves calculated in the ANO-RCC-VQZP/VTZP basis sets for the most stable $^1S_0$ and triplet ($^3D_3$ and $^3F_4$) states of the Pt−Bz complex, with the metal adsorbed at the hollow position. The resulting double-well potential is shown by the black line. Note that the energies of the subsystems used for the calculation of interaction energies correspond to their ground state (i.e., Pt atom, triplet state; benzene molecule, singlet state).

effects for the Pt atom and the complex are similar, which leads to a cancellation in energy differences; the respective stabilization energy is reduced in the energy minimum only by about 4 kcal/mol. The SOC effects for the singlet state of the complex are smaller than for the atom (in the ground triplet state), which leads to the reduction of binding energy by as much as 9.5 kcal/mol. On the other hand, the SOC stabilizes the $^3F_4$ state of the complex, where the increase of the

stabilization energy by about 8 kcal/mol was observed (cf. Figures 2 and 3). These diverse effects of the SOC cause the crossing of the $^3F_4$ state energy curve with the singlet $^1S_0$ and triplet $^3D_3$ state energy curves. Consequently, the second minimum appears at a distance of about 3.2 Å.

We conclude this part by noting that the double-minimum character of the interaction energy curve was detected only at the multireference perturbation theory levels with the inclusion of SOC. In this case, both minima were well separated. The correlated single-reference (MP2 and CCSD(T)) as well as the multireference (CASPT2 and MS-CASPT2) methods provide also two minima (one for the singlet state and one for the triplet state), which are, however, very close to each other. The resulting energy curves are characterized by a single energy minimum (corresponding to the $^1S_0$ state) with a shoulder (coming from crossing of $^1S_0$ and $^3D_3$ states) at greater distances.

The orbital analysis, performed at the CASPT2/VTZP level of theory, indicates the different nature of bonding in differing spin states of the complex. The Pt−Bz complex in the singlet state is characterized by the formation of a dative bond. We should note that the dative bond was also found in the case of the (singlet) Pd−Bz complex.[14] Analyzing the Mulliken charge distributions, we found a direct charge transfer from Pt d orbitals to the π^* molecular orbitals of benzene as well as the backward charge transfer from the π molecular orbitals of the benzene to the s orbitals of the Pt atom. The total charge on the metal atom in Pt−Bz is smaller (0.027e) than the charge in Pd−Bz (0.073e). The bonding in the triplet $^3D_3$ state of the Pt−Bz complex is of similar nature. However, in comparison with the singlet state, the metal atom in the $^3D_3$ state is negatively charged, and the charge is much larger (0.303e). This can be explained by the higher ionization potential of the Pt atom (in comparison with the Pd atom), leading to the damping of the charge transfer from Pt-atom d orbitals and to higher electron affinity, which increases the charge transfer to the s orbital of the Pt atom. The singlet and triplet states are characterized by molecular orbitals formed by a linear combination of the s and d orbitals of the Pt atom with the three highest-occupied π orbitals of the benzene. The higher stability of the complex in the singlet state is explained by a higher orbital mixing. Besides the formation of the dative bond, there exists an additional stabilization contribution—a charge transfer from the benzene to the metal atom. This contribution, found in the $^3F_4$ state of the Pt−Bz, is responsible for the creation of the second minimum. In this case, the metal atom carries a negative charge (0.106e). A similar interaction has recently been observed in Au−Bz complexes.[14]

The interaction energies calculated by pw PBE, PBE+vdW, PBE/EE+vdW are displayed in Figure 4. All xc functionals reproduce the spin-crossing revealed by the WFT methods. The DFT calculations corroborate that the Pt−Bz complex prefers the singlet ground-state at short distances (<2.4 Å), and the spin-crossing occurs at medium Pt−Bz distances (2.4−2.6 Å). The triplet state begins to be favored at longer distances, because the Pt atom approaches its $^3D_3$ ground state. It should be noted that the total energies converge rather badly around the crossing point, which is probably caused by the proximity of the spin states.

In general, the topologies of the calculated DFT potential-energy surface curves are mutually consistent, but the methods differ significantly in the calculated adsorption energies (Table 1). Surprisingly, simple generalized gradient approximation

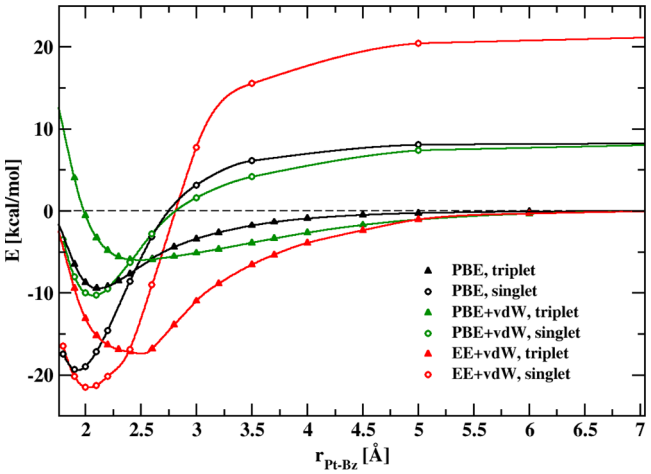

Figure 4. The potential-energy curves calculated by scalar relativistic pw DFT with various vdW terms. The spin state of the Pt atom is fixed to the singlet or triplet multiplicity.

yields the interaction energy of the triplet Pt rather close to the CCSD(T) result. The inclusion of the vdW-DF term brings a positive contribution to the interaction energy; i.e., it leads to a weaker attraction than that predicted by the pure PBE xc functional. A similar effect was observed in the study of the Pd atom over benzene.[14] On the other hand, semiempirical dispersion methods (such as D3 correction by Grimme et al.[53]) are not able to reproduce this behavior, since, by definition, they always provide a negative contribution to the interaction energy, as apparent in Figure 5, reporting the results from the PBE and PBE+D3 calculations involving the Gaussian VQZP basis set.

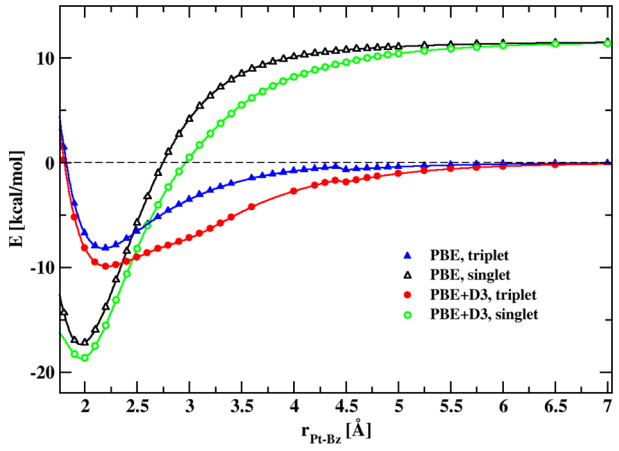

Figure 5. The potential-energy curves calculated by scalar relativistic DFT using the Gaussian def2-VQZP basis set.

The combination of the vdW term with EE (Figure 4) increases the stabilization energy of singlet Pt to 21.5 kcal/mol. This energy is in fact between 13.4 kcal/mol calculated by the CCSD(T) and 36.2 kcal/mol obtained from the CASPT2 method. However, the stabilization energy depends on the description of the $5d^96s^1 \rightarrow 5d^{10}$ excitation energy in the Pt atom, which in turn depends strongly on the xc functional used. This is the reason why the stabilization energy of triplet Pt is overestimated in the EE calculation as compared to the WFT data.

dx.doi.org/10.1021/ct400016c | J. Chem. Theory Comput. 2013, 9, 1461−1468

Figure 6 shows the interaction energy of Pt with benzene calculated with SOC. For large Pt−Bz distance(s), the complex

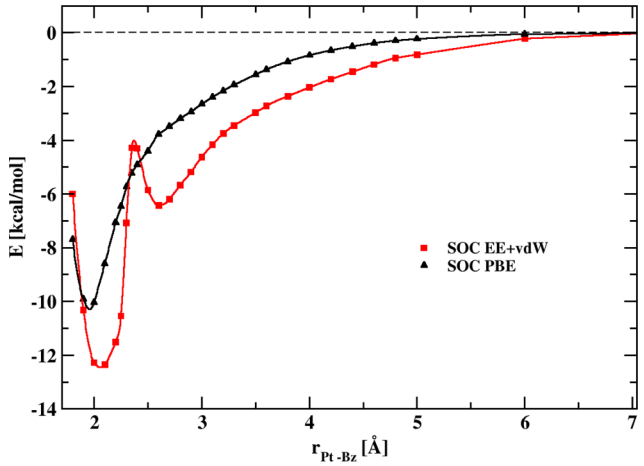

Figure 6. The potential-energy curves calculated by two-component relativistic DFT including spin−orbit coupling calculated by PBE functional and EE+vdW methods. The spin moment of the Pt atom is noncollinear and allowed to relax.

reveals a triplet ground-state multiplicity. As the Pt atom approaches the benzene, the energy of the triplet slowly rises to the transition distance (∼2.6 Å), where the singlet state becomes a ground state. In this case, the transition is associated with the sharp local maximum of the interaction energy, as apparent from Figure 4. The maximum arises from the EE part of the energy, because in the PBE calculation, which includes SOC, there is no such local maximum. Notice that EE gives much larger triplet−singlet excitation energy for the isolated Pt atom than pure PBE (see the dissociation limit in Figure 4 and Table 1). This difference may be responsible for the maximum; the EE is evaluated on a set of Kohn−Sham orbitals, which are preconverged using the PBE functional. The lower excitation energy in PBE causes the transition to the singlet state to occur at Pt−Bz distances, at which the EE still prefers the triplet state. That generates the energy penalty, which results in a sudden increase of the interaction energy near the point of spin-crossing.

The results also demonstrate some of the weaknesses of the DFT calculations. Although the double minimum shape of the energy in Figure 6 roughly resembles the CASPT2-SO curves, it partly arises from the unphysical behavior of the method, as discussed in the preceding paragraph. Moreover, it is not possible to unveil the symmetry of the states to examine whether the second minimum comes from the intermixing of the $^3D_3$ and $^3F_4$ states, which was observed in the MS-CASPT2 calculations including SOC. Similarly, a comparison of the open-shell and closed-shell singlet states is not possible within the DFT either due to its single-reference character. These limitations underline the advantages of multireference WFT approaches (such as CASPT2), which can describe the true nature of bonding in such complexes in a more rigorous way.

As already pointed out, the Pt−Bz interaction energies at the HF level are repulsive along the whole potential-energy surfaces, for both the singlet and triplet states (Figure 1). This suggests that the stability of the complex (at the scalar relativistic level) arises mainly from the dynamic correlation effects. The QMC method is especially relevant in such circumstances. We have therefore performed large-scale QMC calculations, scanning the whole Pt−Bz distance coordinate. Trial wave functions were constructed using two modern xc functionals, TPSSh and M11. The obtained results were compared against CCSD(T), used as a reference (Figure 7), in order to assess the performance of the QMC approach considered.

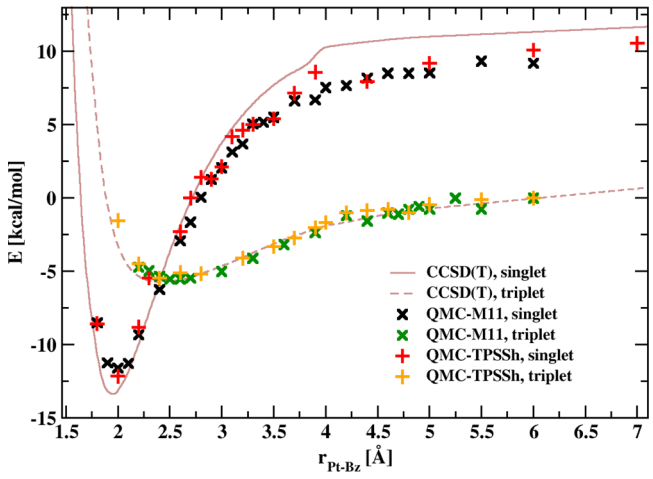

Figure 7. A comparison of the potential-energy surfaces from Quantum Monte Carlo (QMC) using M11 (QMC-M11) and TPSSh (QMC-TPSSh) trial wave functions vs CCSD(T)/VTZP data. The QMC error bars are smaller than the symbol line width.

For the triplet state, aligned to zero at the dissociation limit, the QMC-M11 and QMC-TPSSh data are indistinguishable and well overlap the CCSD(T) curve. In the singlet state, the QMC-TPSSh results follow remarkably well the CCSD(T) data in the bonding region around the minimum and in the dissociation limit (cf. Table 1). The reason for the slightly lower energy at medium distances (3−6 Å, Figure 7) is hard to assess. It may be tentatively attributed to the presence of an explicit interelectronic dependence, improving the description of short-range correlations, but the effect of neglecting the multireference character is not clear. The QMC-M11 approach performs considerably worse than QMC-TPSSh. For instance, the deviation in the interaction energy, with respect to CCSD(T), achieves nearly 2 kcal/mol (Table 1). The discrepancy may be attributed to a larger fixed-node error of the respective M11 trial wave functions when compared to the TPSSh ones.

The reported QMC potentials, obtained along the whole Pt−Bz distance region of interest, for closed-shell singlet and triplet states, suggest a viable use of the TPSSh trial wave functions. Their use may be beneficial in future large-scale QMC calculations of the related Pt-containing organometallic systems, where CCSD(T) is out of reach due to its rapid cost scaling.

CONCLUSIONS

In summary, we report and analyze the interaction between benzene and a Pt atom using a wide range of methods, including WFT, DFT, and QMC. Concerning the nature of the bonding, the character of the adsorption of the Pt atom on the benzene molecule is determined by three different effects. First, the electronic state of the Pt atom changes upon its interaction with the benzene from the ground triplet state ($^3D_3$), which is characteristic for an isolated Pt atom, to the closed-shell singlet

dx.doi.org/10.1021/ct400016c | J. Chem. Theory Comput. 2013, 9, 1461−1468

state ($^1S_0$) when bound to the benzene. Second, the orbital analysis shows an overlap of the d orbital of the Pt atom with the π molecular orbitals of the benzene, which are primarily responsible for the stability of the complex. Third, the forward and backward charge transfer between the Pt metal atom and the benzene was identified in the bonding. Consequently, the interaction between the Pt metal atom and the benzene can be characterized as a formation of a so-called dative bond. This explains the high stability and short bond distances of the complex in the singlet $^1S_0$ state. The Pt atom in the triplet state ($^3D_3$) is bound to the benzene molecule also by a dative bond. However, while the charge on the metal atom is positive in the singlet state of the complex, the triplet state induces a negative charge.

The single-reference CCSD(T) and MP2 methods as well as the multireference CASPT2 method and its extension MS-CASPT2 provide the double-minimum energy curve, where these two minima (one for the singlet state and one for the triplet state) are very close together and almost overlap. The resulting energy curves are characterized by a single energy minimum (corresponding to the $^1S_0$ state) with a shoulder (from the crossing between the $^1S_0$ and $^3D_3$ states) at longer distances. The inclusion of SOC leads to an appearance of a second shallow but well-separated minimum, which corresponds to the triplet state ($^3F_4$) of the Pt−Bz complex. The bonding in this state is characterized by a strong charge transfer from the benzene to the Pt metal atom.

DFT methods are suitable for a qualitative description of the general potential-surface features, including the prediction of the single minima on the singlet and triplet and on the minimum energy interaction curves, minimum positions, and spin-crossing. In this respect, PBE/EE+vdW is found to match CCSD(T) results. The stabilization energies vary strongly depending on the choice of the xc functional and dispersion correction. The inclusion of SOC at the DFT level lowers the stabilization energies. The incorporation of EE correction in the SOC calculation induces the formation of the second weak minimum on the interaction curve, which is however attributed to an artifact of the method used: the exact exchange evaluated on a set of Kohn−Sham orbitals obtained from the previous PBE calculation. These results demonstrate how difficult the interpretation of the DFT data calculated with various nonlocal functionals may be without prior benchmarking.

CCSD(T) confirms the existence of single minima on both the singlet and triplet minimum energy potential-surface scans at the scalar-relativistic level. As compared to the experiment, it describes well the *j*-averaged $^1S-^3D$ splitting of the Pt atom at the dissociation limit. In addition, CCSD(T) serves well as a guide for an assessment of the QMC trial wave function quality. Full Pt−Bz interaction QMC curves were obtained for two types of the trial wave functions from DFT, using M11 and TPSSh xc functionals. The QMC-TPSSh protocol reveals favorable agreement with the reference data, allowing its use in future large-scale calculations of the related organometallic compounds.

AUTHOR INFORMATION

Corresponding Author

*E-mail: michal.otyepka@upol.cz; pavel.hobza@uochb.cas.cz.

Author Contributions

‖Both authors contributed equally to this work

Notes

The authors declare no competing financial interest.

ACKNOWLEDGMENTS

The authors gratefully acknowledge the support from the Operational Program Research and Development for Innovations−European Regional Development Fund (projects CZ.1.05/2.1.00/03.0058 of the Ministry of Education, Youth and Sports of the Czech Republic), the Operational Program Education for Competitiveness−European Social Fund (projects CZ.1.07/2.3.00/20.0017 and CZ.1.07/2.3.00/30.0004 of the Ministry of Education, Youth and Sports of the Czech Republic), and the Czech Science Foundation (projects P208/12/G016 and P208/10/1742). This work was part of the Research Project RVO: 61388963 of the Institute of Organic Chemistry and Biochemistry, Academy of Sciences of the Czech Republic. The support of Praemium Academiae of the Academy of Sciences of the Czech Republic, awarded to P.H. in 2007, is also acknowledged. M.D. acknowledges the allocation at the National Supercomputing Infrastructure, Computing Center of the Slovak Academy of Sciences, supported from the structural funds of EU.

REFERENCES

(1) Syomin, D.; Kim, J.; Koel, B. E.; Ellison, G. B. *J. Phys. Chem. B* **2001**, *105*, 8387−8394.
(2) Nieminen, V.; Honkala, K.; Taskinen, A.; Murzin, D. Y. *J. Phys. Chem. C* **2008**, *112*, 6822−6831.
(3) Ago, H.; Ogawa, Y.; Tsuji, M.; Mizuno, S.; Hibino, H. J. *Phys. Chem. Lett.* **2012**, *3*, 2228−2236.
(4) Heath, J. R.; Ratner, M. A. *Phys. Today* **2003**, *56*, 43−49.
(5) Cho, W. J.; Cho, Y.; Min, S. K.; Kim, W. J.; Kim, K. S *J. Am. Chem. Soc.* **2011**, *133*, 9364−9369.
(6) Cho, Y.; Choi, Y. C.; Kim, K. S. *J. Phys. Chem. C* **2011**, *115*, 6019−6023.
(7) Jenkins, S. J. *Proc. R. Soc. London, Ser. A* **2009**, *465*, 2949−2976.
(8) Tonigold, K.; Groß, A. *J. Chem. Phys.* **2010**, *132*, 224701.
(9) Grimme, S. *Mol. Sci.* **2011**, *1*, 211−228.
(10) Cohen, A. J.; Mori-Sanchez, P.; Yang, W. *Chem. Rev.* **2012**, *112*, 289−320.
(11) Dion, M.; Rydberg, H.; Schröder, E.; Langreth, D. C.; Lundqvist, B. I. *Phys. Rev. Lett.* **2004**, *92*, 246401.
(12) Ruiz, V. G.; Liu, W.; Zojer, E.; Scheffler, M.; Tkachenko, A. *Phys. Rev. Lett.* **2012**, *108*, 146103.
(13) Liu, W.; Carrasco, J.; Santra, B.; Michaelides, A.; Scheffler, M.; Tkachenko, A. *Phys. Rev. B* **2012**, *86*, 245405.
(14) Granatier, J.; Lazar, P.; Otyepka, M.; Hobza, P. *J. Chem. Theory Comput.* **2011**, *7*, 3743−3755.
(15) Granatier, J.; Lazar, P.; Prucek, R.; Šafárová, K.; Zboril, R.; Otyepka, M.; Hobza, P. *J. Phys. Chem. C* **2012**, *116*, 14151−14162.
(16) Ihm, H.; Ajo, H. M.; Gottfried, J. M.; Bera, P.; Campbell, C. T. *J. Phys. Chem. B* **2004**, *108*, 14627−14633.
(17) Roszak, S.; Balasubramanian, K. *Chem. Phys. Lett.* **1995**, *234*, 101−106.
(18) Majumdar, D.; Roszak, S.; Balasubramanian, K. J. *Chem. Phys.* **2001**, *114*, 10300.
(19) Youn, I. S.; Kim, D. Y.; Singh, N. J.; Park, S. W.; Youn, J.; Kim, K. S. *J. Chem. Theory Comput.* **2012**, *8*, 99−105.
(20) Rosillo, M.; Dominguez, G.; Perez-Castells, J. *Chem. Soc. Rev.* **2007**, *36*, 1589−1604.
(21) Polestshuk, P. M.; Dem'yanov, P. I.; Ryabinkin, I. G. *J. Chem. Phys.* **2008**, *129*, 054307.
(22) Zohuri, G. H.; Albahily, K.; Schwerdtfeger, E. D.; Miller, S. A. *Polymer Science: A Comprehensive Reference*; Elsevier Science: New York, 2012; Vol. 3, pp 673−697.
(23) Jin, P.; Li, F.; Chen, Z. *J. Phys. Chem. A* **2011**, *115*, 2402−2408.

(24) Yi, H. B.; Diefenbach, M.; Choi, Y. C.; Lee, E. C.; Lee, H. M.; Hong, B. H.; Kim, K. S. *Chem.—Eur. J.* **2006**, *12*, 4885−4892.
(25) Miyajima, K.; Nakajima, A.; Yabushita, S.; Knickelbein, M. B.; Kaya, K. *J. Am. Chem. Soc.* **2004**, *126*, 13202−13203.
(26) Xiang, H.; Yang, J.; Hou, J. G.; Zhu, Q. *J. Am. Chem. Soc.* **2006**, *128*, 2310−2314.
(27) Błoński, P.; Hafner, J. *J. Chem. Phys.* **2011**, *134*, 154705.
(28) Błoński, P.; Hafner, J. *J. Chem. Phys.* **2012**, *136*, 074701.
(29) Sansonetti, J. E.; Martin, W. C. *J. Phys. Chem. Ref. Data* **2005**, *34*, 1559−2259.
(30) Horváthová, L.; Dubecký, M.; Mitas, L.; Štich, I. *Phys. Rev. Lett.* **2012**, *109*, 053001.
(31) Daku, L. M. L.; Aquilante, F.; Robinson, T. W.; Hauser, A. *J. Chem. Theory Comput.* **2012**, *8*, 4216−4231.
(32) Ma, J.; Alfè, D.; Michaelides, A.; Wang, E. *J. Chem. Phys.* **2009**, *130*, 154303.
(33) Neogrády, P.; Urban, M. *Int. J. Quantum Chem.* **1995**, *55*, 187.
(34) Neogrády, P.; Urban, M.; Hubač, I. In *Recent Advances in Coupled-Cluster Methods*; Bartlett, R. J., Ed.; World Scientific: Singapore, 1997; p 275.
(35) Watts, J. D.; Gauss, J.; Bartlett, R. J. *J. Chem. Phys.* **1993**, *98*, 8718.
(36) Heckert, M.; Heun, O.; Gauss, J.; Szalay, P. G. *J. Chem. Phys.* **2006**, *124*, 124105.
(37) Møller, C.; Plesset, M. S. *Phys. Rev.* **1934**, *46*, 0618.
(38) Roos, B. O. In *Advances in Chem. Phys.; Ab Initio Methods in Quantum Chemistry - II*; Lawley, K. P., Ed.; John Wiley & Sons Ltd.: Chichester, England, 1987; p 399.
(39) Andersson, K.; Malmqvist, P.-Å.; Roos, B. O.; Sadlej, A. J.; Wolinski, K. *J. Phys. Chem.* **1990**, *94*, 5483.
(40) Andersson, K.; Malmqvist, P.-Å.; Roos, B. O. *J. Chem. Phys.* **1992**, *96*, 1218.
(41) Roos, B. O.; Andersson, K.; Fülscher, M. P.; Malmqvist, P.-Å.; Serrano-Andrés, L.; Pierloot, K.; Merchán, M. In *Advances in Chemical Physics: New Methods in Computational Quantum Mechanics*; Prigogine, I., Rice, S. A., Eds.; John Wiley & Sons: New York, 1996; Vol. *XCIII*, pp 219−331.
(42) Finley, J.; Malmqvist, P. Å.; Roos, B. O.; Serrano-Andrés, L. *Chem. Phys. Lett.* **1998**, *288*, 299−306.
(43) Ghigo, G.; Roos, B. O.; Malmqvist, P.-Å *Chem. Phys. Lett.* **2004**, *396*, 142.
(44) Roos, B. O.; Malmqvist, P.-Å. *Adv. Quantum Chem.* **2004**, *47*, 37.
(45) Roos, B. O.; Malmqvist, P.-Å. *Phys. Chem. Chem. Phys.* **2004**, *6*, 2919.
(46) Iliaš, M.; Kellö, V.; Urban, M. *Acta Phys. Slov.* **2010**, *60*, 259−391.
(47) Roos, B. O.; Lindh, R.; Malmqvist, P. Å.; Veryazov, V.; Widmark, P. O. *J. Phys. Chem. A* **2004**, *108*, 2851.
(48) Roos, B. O.; Lindh, R.; Malmqvist, P. Å.; Veryazov, V.; Widmark, P. O. *J. Phys. Chem. A* **2005**, *109*, 6575.
(49) Douglas, M.; Kroll, N. M. *Ann. Phys.* **1974**, *82*, 89.
(50) Hess, B. A.; Chandra, P. *Phys. Scr.* **1987**, *36*, 412.
(51) Boys, S. F.; Bernardi, F. *Mol. Phys.* **1970**, *19*, 553.
(52) Karlström, G.; Lindh, R.; Malmqvist, P. Å.; Roos, B. O.; Ryde, U.; Veryazov, V.; Widmark, P. O.; Cossi, M.; Schimmelpfennig, B.; Neogrády, P.; Seijo, L. *Comput. Mater. Sci.* **2003**, *28*, 222.
(53) Grimme, S.; Antony, J.; Ehrlich, S.; Krieg, H. *J. Chem. Phys.* **2010**, *132*, 154104.
(54) Weigend, F.; Ahlrichs, R. *Phys. Chem. Chem. Phys.* **2005**, *7*, 3297−3305.
(55) Perdew, J. P.; Burke, K.; Ernzerhof, M. *Phys. Rev. Lett.* **1996**, *77*, 3865.
(56) Perdew, J. P.; Burke, K.; Ernzerhof, M. *Phys. Rev. Lett.* **1997**, *78*, 1396.
(57) Schmidt, M. W.; Baldridge, K. K.; Boatz, J. A.; et al. *J. Comput. Chem.* **1993**, *14*, 1347.
(58) Blochl, P. E. *Phys. Rev. B* **1994**, *50*, 17953.
(59) Kresse, G.; Joubert, D. *Phys. Rev. B* **1999**, *59*, 1758.
(60) Dubecký, M.; Derian, R.; Mitas, L.; Štich, I. *J. Chem. Phys.* **2010**, *133*, 244301.
(61) Dubecký, M.; Derian, R.; Horváthová, L.; Allan, M.; Štich, I. *Phys. Chem. Chem. Phys.* **2011**, *13*, 20939−20945.
(62) Tao, J. M.; Perdew, J. P.; Staroverov, V. N.; Scuseria, G. E. *Phys. Rev. Lett.* **2003**, *91*, 146401.
(63) Peverati, R.; Truhlar, D. G. *J. Phys. Chem. Lett.* **2011**, *2*, 2810−2817.
(64) Greeff, C.; Lester, W. A., Jr. *J. Chem. Phys.* **1998**, *109*, 1607.
(65) Ovcharenko, I.; Aspuru-Guzik, A.; Lester, W. A., Jr. *J. Chem. Phys.* **2001**, *114*, 7790.
(66) Dunning, J. T. H. *J. Chem. Phys.* **1989**, *90*, 1007.
(67) Andrae, D.; Haeussermann, U.; Dolg, M.; Stoll, H.; Preuss, H. *Theor. Chem. Acc.* **1990**, *77*, 123−141.
(68) Moskowitz, J. W.; Schmidt., K. E. *J. Chem. Phys.* **1992**, *97*, 3382−3385.
(69) Bajdich, M.; Mitas, L. *Acta Phys. Slov.* **2009**, *59*, 81−168.
(70) Grimm, R. C.; Storer, R. G. *J. Comput. Phys.* **1971**, *7*, 134.
(71) Anderson, J. B. *J. Chem. Phys.* **1975**, *63*, 1499.
(72) Anderson, J. B. *J. Chem. Phys.* **1976**, *65*, 4121.
(73) Wagner, L.; Bajdich, M.; Mitas, L. *J. Comput. Phys.* **2009**, *228*, 3390 http://www.qwalk.org.
(74) Hopkins, B. W.; Tschumper, G. S. *J. Phys. Chem. A* **2004**, *108*, 2941−2948.
(75) Riley, K. E.; Pitoňák, M.; Jurečka, P.; Hobza. *P. Chem. Rev.* **2010**, *110*, 5023−5063.
(76) Blaise, J.; Vergés, J.; Wyart, J.-F.; Engleman, R., Jr. *J. Res. Natl. Inst. Stand. Tech.* **1992**, *97*, 213.